Basin Research (2008) doi: 10.1111/j.1365-2117.2008.00368.x

Quantifying geomorphology associated with large subduction zone earthquakes

Eugene C. Morgan,* Brian G. McAdoo† and Laurie G. Baise*

*Department of Civil and Environmental Engineering, Tufts University, Medford, MA, USA
†Department of Earth Science and Geography, Vassar College, Poughkeepsie, NY, USA

ABSTRACT

For 30 large-earthquake generating subduction zones, we quantify forearc basin size and subducting seafloor roughness to see if the size and shape of geomorphologic features determine earthquake magnitude. The subduction of geomorphologic features, such as ridges and seamounts, not only influences seismicity, but increases basal erosion and subsidence of the accretionary wedge, resulting in the formation of forearc basins. Many subduction zone ruptures have been associated with these basins, where a great portion of the ruptures' asperities collocate with the basins. First, we attempt to discern a relationship between forearc and subducting geomorphology by quantifying along-strike variations in the bathymetry associated with 30 different rupture zones and the sections of subducting seafloor adjacent to those rupture zones. Two parameters, determined from theoretical models fit to empirical semivariograms, characterize areas of bathymetry: the sill, which estimates the degree of relief in the terrain, and the range, which is the horizontal scale associated with the sill. The ratio of sill to range provides us with a measure of seafloor roughness at a scale relevant to the mechanics of subduction. We investigate the control that forearc basins and subducting bathymetric highs may have on the occurrence of large thrust earthquakes by separately comparing our rupture zone and subducting seafloor roughness measurements to the moment magnitudes of the 30 events. The trench-parallel dimension of bathymetrically high features on the subducting seafloor appears to correlate with moment magnitude. Also, we observe in the ratio of sill to range measurements that geomorphology on the subducting seafloor and forearc constrain the earthquake size at a margin.

INTRODUCTION

The world's largest earthquakes occur at subduction zones, where subducting oceanic plates form thrust faults with overriding plates (Kanamori, 1986). Previous studies have observed along-trench variations in earthquake occurrence (Tanioka *et al*., 1997; Bilek, 2007), and suggest the possibility that the morphology of the subducting seafloor affects rupture dynamics (Mogi, 1969; Kanamori & Kikuchi, 1993). Significant features, such as seamounts (Cloos, 1992; Cloos & Shreve, 1996), ridges (Spence *et al*., 1999; Bilek *et al*., 2003), and horst and graben structures (Tanioka *et al*., 1997), affect coupling at the subduction zone interface, and potentially result in subduction erosion and basin formation (von Huene & Scholl, 1991). Thicker sediments on the subducting plate may decrease seismicity (Byrne *et al*., 1988), or increase it when burying seamounts, as found in Chilean-type margins (Cloos & Shreve, 1996). All of these factors attributing to variations in seismicity express themselves geomorphologically, and such morphology can be analyzed quantitatively (Goff *et al*., 1999; McAdoo *et al*., 2004).

Correspondence: Eugene C. Morgan, Department of Civil and Environmental Engineering, Tufts University, 200 College Ave., Anderson Hall, Rm. 113, Medford, MA 02155, USA. E-mail: eugene.morgan@tufts.edu

The roughness of the subducting seafloor not only affects seismicity, but also affects forearc geomorphology, and forearc geomorphology itself may have implications in subduction zone rupture dynamics. Song & Simons (2003) observe more frequent and larger earthquakes at margins possessing strongly negative trench-parallel gravity anomalies (TPGA) and topography anomalies (TPTA). For large circum-Pacific megathrust earthquakes, areas of high coseismic slip (asperities) are generally collocated with forearc basins and gravity lows (Wells *et al*., 2003). These basins may originate from subduction erosion at the base of the forearc (von Huene & Scholl, 1991), cumulative interseismic subsidence (Sugiyama, 1994), the downward motion of the lower plate (Mogi, 1969), or strong forearc crust at depth, where the growing accretionary wedge traps sediment behind it (Byrne *et al*., 1988). Large amounts of subsidence have been attributed to basal erosion (von Huene & Scholl, 1991), and the subduction of seamounts and ridges generate greater rates of erosion and basin-specific subsidence (Laursen *et al*., 2002). Therefore, rougher subducting seafloor should generate rougher forearc with larger basins.

Subduction zone seismicity can be related to both forearc and subducting seafloor geomorphology. Cloos (1992) correlates earthquake moment magnitude to the height of subducting seamounts, and finds that seamount diameters are comparable to the diameters of asperities. Cloos (1992)

and Cloos & Shreve (1996) proposed that successive ruptures occur as a result of stick-slip shearing at the bases of these basaltic seamounts as they collide with the 'backstops' at the arcward edge of the accretionary prisms. This view concurs with the idea that areas of high shear strength between the overriding and subducting plates control earthquake recurrence at subduction margins (Thatcher, 1990). Earthquakes nucleate at these high-shear-strength centers, and spread according to conditions in interspersed weak zones. Apart from acting as asperities, these bathymetric highs may serve as significant agents of basal erosion beneath the forearc, possibly resulting in the formation of basins. In areas where subsidence data are available, Wells *et al.* (2003) observe a coincidence between the locus of subduction erosion and the source zone of large earthquakes. Fuller *et al.* (2006) explains the tendency of earthquakes to occur under forearc basins with stable wedges that may aid in thermal pressurization, expedite loading, and increase healing of the fault. Increases in TPGA towards the outer limits of rupture zones indicate that heterogeneous physical conditions limit rupture propagation (Llenos & McGuire, 2007). Also, rigidity of rock and sediment involved in these ruptures may vary up to a factor of 5 (Bilek & Lay, 1999). Many of these studies suggest that differences in subduction zone ruptures can be attributed, at least partly, to along-strike geomorphological variation of the forearc (result) or the subducting seafloor (agent).

This study aims to determine how the size of forearc basins and the roughness of subducting seafloor may control the seismic hazard at a given margin, and how they may affect each other. In particular, our analysis concerns the distribution of large earthquake events at given subduction zones. By constructing semivariograms for the bathymetry associated with 30 large rupture zones and their neighboring subducting seafloor, we systematically obtain quantitative characteristics of the morphology associated with these ruptures. We compare subducting seafloor roughness to rupture zone roughness, and both of these measurements to earthquake magnitude.

METHODS

Data selection

In order to investigate any potential relationship between geomorphology and earthquake size, we started by selecting 30 subduction earthquakes with $M_w > 7.5$ (Tables 1 and 2). We attempted to select historically maximum earthquakes, and so we do not claim to use the maximum possible magnitudes at any given margin in our study. Selection of these events was largely based upon availability of rupture zone data, specifically geographic orientation, which came from Wells *et al.* (2003) and the USGS National Earthquake Information Center (http://earthquake.usgs.gov/regional/neic/). The National Geophysical Data Center (NGDC; http://www.ngdc.noaa.gov/ngdc.html) provided all moment magnitude values, except for the 1700 Cascadia magnitude, which came from Satake *et al.* (2003). In selecting events, we tried to maintain a broad geographic distribution in order to diversify the regional landscapes sampled for bathymetry data (Fig. 1).

Bathymetric maps from the Smith and Sandwell global topography data (V9.1b) display these rupture zones by region, and these data serve as the source for all geostatistical analyses presented in this study (Smith & Sandwell, 1997). The Smith and Sandwell data set provides global coverage at the highest available resolution (1-min grid point spacing), but unlike the GEBCO data set (also 1-min resolution), the Smith and Sandwell data set uses satellite gravity measurements and available depth soundings to predict depth data points on the 1-min grid. We believe that this method gives more consistent and accurate global topography than the GEBCO data set, because the GEBCO data interpolates digitized ship tracklines with a spline algorithm. Because this study compares statistics of different geographic regions, it is necessary to use data of uniform quality and resolution for all of the study areas, and so we did not seek higher resolution data sets (e.g. multibeam) for each rupture zone.

We subset the Smith and Sandwell global topography to areas encompassing each rupture zone using Generic Mapping Tools (GMT) commands (available with the Smith and Sandwell data set). For each area, a Lambert projection converted the latitude-longitude grid to matrices of x- and y-coordinates so that the depth data points were separated by real distances (i.e. meters). In order to sample the bathymetry of the subducting seafloor, we constructed polygons that mirror the rupture zones in dimension (Figs 2 and 3, left panels). These polygons extend away from the trench in the opposite direction of plate motion. Sampling the subducting seafloor in this manner assumes that the seafloor that is about to be subducted has similar roughness to the seafloor that currently underlies the forearc. This assumption likely holds true for linear features, such as ridges, faults, and seamount chains oriented non-parallel to the trench axis, but for other features, such as individual seamounts or linear features parallel to the trench, this assumption is debatable because their continuity is difficult to establish from bathymetry data alone.

Semivariogram analysis

Semivariance serves as an adequate tool for characterizing surfaces. For example, previous studies have employed semivariance to describe seafloor roughness (Bell, 1979), glacier morphology (Bishop *et al.*, 2003), landslide roughness (Glenn *et al.*, 2006), and topography (Sung & Chen, 2004). Semivariance describes the spatial correlation of the bathymetry by measuring variance of depth as a function of the distance separating depth data points. In terms of bathymetry and topography (x, y, z data), it averages the squared difference in elevation (z) between pairs of datum (at points defined by x and y, or just x, as in

Table 1. Data from rupture zone semivariogram analysis

Event	M_w	Rupture area (km^2)	Sample area (km^2)	Sill (km^2)	Range (km)	κ	L_{max} (km)	Sum of squares (km^4)
1968 Hyuga-nada	7.8	2149	5619	0.33	74	1	91	122
1923 Kanto	7.9	5595	9323	0.1	80	1	186	32
1995 Jalisco	8	8125	16 153	0.28	119	0.99	190	125
1971 Chile	7.8	9944	20 296	0.25	63	1	167	144
1946 Unimak Is.	8.3	10 911	24 067	0.14	56	1	157	110
1985 Michoacan	8.1	12 003	20 914	0.22	109	1	245	130
1958 Kurile Is.	8.3	12 825	23 937	0.29	207	1	253	9689
2007 Solomon Is.	8.1	13 325	25 977	0.96	85	1	385	4316
1968 Hokkaido	8.3	15 160	39 699	0.52	186	1	220	2992
1985 Valparaiso, Chile	8	16 372	35 560	0.36	143	0.97	324	4839
1943 Chile	7.8	17 238	36 109	0.32	124	0.66	390	472
1992 Nicaragua	7.7	17 245	33 422	0.88	266	1	287	62 271
1963 Kurile Is.	8.5	18 310	32 331	0.33	48	1	370	549
1973 Hokkaido	7.8	20 248	36 029	0.26	240	1	324	268
1923 Kamchatka	8.5	21 183	43 580	1.03	87	1	270	147 812
1969 Kurile Is.	8.2	23 657	42 472	0.49	292	1	370	104 693
1952 Hokkaido	8.4	23 858	46 939	0.81	259	1	249	153 327
1944 Nankai	8.1	31 640	60 744	0.31	93	1	285	229
2006 Java	7.7	31 999	55 260	1.31	328	1	535	60 838
1946 Nankai	8.3	33 512	69 558	0.31	97	1	421	2053
1952 Kamchatka	9	42 115	85 861	0.88	107	1	438	183 278
1938 Kodiak Is.	8.3	47 492	93 580	0.1	284	0.9	557	3309
1965 Rat Is.	8.7	50 443	100 031	2.54	237	1	1028	7 802 460
2005 Sumatra	8.7	58 854	112 817	0.49	225	1	735	8248
1700 Cascadia	9	61 957	98 382	0.26	128	1	1378	2690
1960 south Chile	9.5	133 541	248 458	0.64	396	1	1463	27 245
1833 Sumatra	8.2	145 884	243 390	2.39	792	1	1334	3 070 410
1964 Prince William	9.2	172 033	264 507	0.39	121	1	1067	29 258
1957 Andreanof Is.	8.6	208 583	395 679	5.86	590	1	1466	326 558 981
2004 Sumatra	9	259 991	361 218	0.74	238	0.73	1637	2 210 254

Eqn. (1) below and in Fig. 4) separated by increasing increments of distance, known as lag distance (L). Smooth seafloor will have low semivariance values, even at large lag distances, whereas rough seafloor will have an initial increase in semivariance that reaches a plateau or maximum value at a relatively short lag distance [compare Figs 2 and 3 for smooth and rough terrain, respectively (discussed in 'Results' section)]. That plateau is termed the sill, and represents the characteristic variance associated with the features causing the roughness of the surface. In terms of bathymetry, the sill can be thought of as an estimate of the degree of relief, because landscapes with greater relief will have larger sills. The lag distance at which 95% of the sill is reached is called the range, and signifies the horizontal scale of maximum variance. The nugget, defined as the semivariance at $L = 0$, may reflect noise in the data or variability at a scale smaller than the sampling resolution. To construct a semivariogram, semivariance (γ) is calculated for every pair of points and binned by L according to:

$$\gamma(L) = \frac{1}{2N(L)} \sum_{i=1}^{N(L)} [z(x_i + L) - z(x_i)]^2 \quad (1)$$

where $N(L)$ is the number of data point pairs of z separated by the values of L in each bin. The semivariogram plots $\gamma(L)$ vs. the midpoint of each bin (i.e. the mean of the range of L for each bin) (Carr & Benzer, 1991; Carr, 1995, 1997).

The semivariogram analyses are carried out on the data points confined to 'sample areas', which consist of the rupture zones and subducting seafloor polygons expanded symmetrically in a direction parallel to the trench by a factor of 2 (e.g. sample areas in Figs 2 and 3). The use of the sample areas allows the lag distances to exceed the rupture zone and subducting seafloor polygon lengths while restricting sampling of the bathymetry data to the forearc (for the rupture zone calculations) and to the near-trench seafloor (for the subducting seafloor calculations). At lag distances approaching the dimensions of the sample area, the number of point pairs becomes critically low, and the values of semivariance become unreliable. Therefore, if the maximum lag distance is equal to or less than the rupture length, the true range and sill cannot be found reliably, if at all, for those rupture zones confined to basins. For all semivariograms, we used maximum lag distances (L_{max}) approximately 1.5 times larger than the lengths of the rupture zones.

To characterize the roughness of the forearc above the rupture zones and that of the subducting seafloor, we applied the semivariance equation (Eqn. 1) to the resi-

Table 2. Data from subducting seafloor semivariogram analysis

Event	M_w	Rupture area (km^2)	Sample area (km^2)	Sill (km^2)	Range (km)	κ	L_{max} (km)	Sum of squares (km^4)
1968 Hyuga-nada	7.8	2149	8789	0.04	70	1	91	3
1923 Kanto	7.9	5595	9224	0.44	33	1	186	1378
1995 Jalisco	8	8125	15 646	0.11	42	1	190	2
1971 Chile	7.8	9944	21 917	0.18	118	1	167	18
1946 Unimak Is.	8.3	10 911	21 018	0.04	10	0.15	157	39
1985 Michoacan	8.1	12 003	23 699	0.15	113	1	245	187
1958 Kurile Is.	8.3	12 825	26 097	0.05	74	1	253	2
2007 Solomon Is.	8.1	13 325	31 309	1.49	399	1	385	1 214 876
1968 Hokkaido	8.3	15 160	23 731	0.23	49	1	220	76
1985 Valparaiso, Chile	8	16 372	36 656	0.23	277	0.89	324	489
1943 Chile	7.8	17 238	42 622	0.09	275	0.83	390	274
1992 Nicaragua	7.7	17 245	21 334	0.39	221	1	287	6188
1963 Kurile Is.	8.5	18 310	39 295	0.44	294	1	370	21 285
1973 Hokkaido	7.8	20 248	27 780	0.13	40	1	324	28
1923 Kamchatka	8.5	21 183	36 592	0.86	138	1	270	154 095
1969 Kurile Is.	8.2	23 657	48 905	0.16	242	1	370	415
1952 Hokkaido	8.4	23 858	27 816	0.31	64	1	249	205
1944 Nankai	8.1	31 640	29 903	0.52	120	1	285	3825
2006 Java	7.7	31 999	59 671	0.27	45	1	535	562
1946 Nankai	8.3	33 512	49 334	0.02	47	0.34	421	1
1952 Kamchatka	9	42 115	80 399	0.52	171	1	438	24 649
1938 Kodiak Is.	8.3	47 492	100 484	0.26	560	0.82	557	215 481
1965 Rat Is.	8.7	50 443	106 533	0.69	192	1	1028	119 759
2005 Sumatra	8.7	58 854	104 580	0.14	140	0.88	735	1767
1700 Cascadia	9	61 957	89 576	0.15	186	0.99	1378	5081
1960 south Chile	9.5	133 541	199 781	0.2	639	0.97	1463	57 342
1833 Sumatra	8.2	145 884	190 835	0.17	144	1	1334	577
1964 Prince William	9.2	172 033	149 729	0.16	282	1	1067	2904
1957 Andreanof Is.	8.6	208 583	242 372	0.04	22	1	1466	21
2004 Sumatra	9	259 991	249 398	0.09	384	0.48	1637	15 777

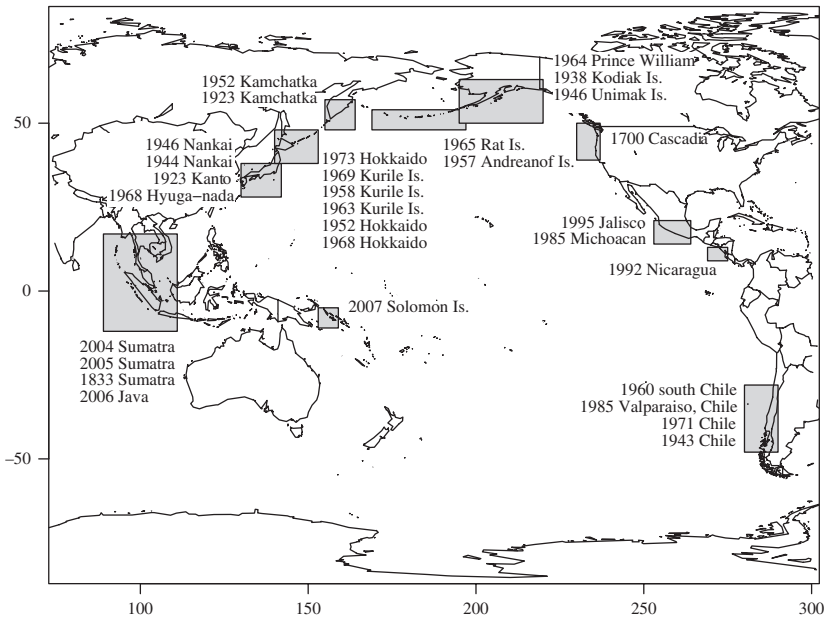

Fig. 1. The global distribution of subduction zone earthquakes used in this study. Events are grouped into regions, marked with gray rectangles, for display purposes only.

duals of a plane fit to the bathymetry data within each sample area. Because we treat the bathymetry that we are measuring as a stochastic surface, it is necessary to use these residuals (i.e. detrend the data) in order to ensure stationarity (spatial homogeneity of the statistics of the stochastic surface) in the data used for the modeling (Goff & Jordan, 1988). Without using the residuals, large-scale trends in the bathymetry pervade the semivariance and

 Basin Research, 10.1111/j.1365-2117.2008.00368.x

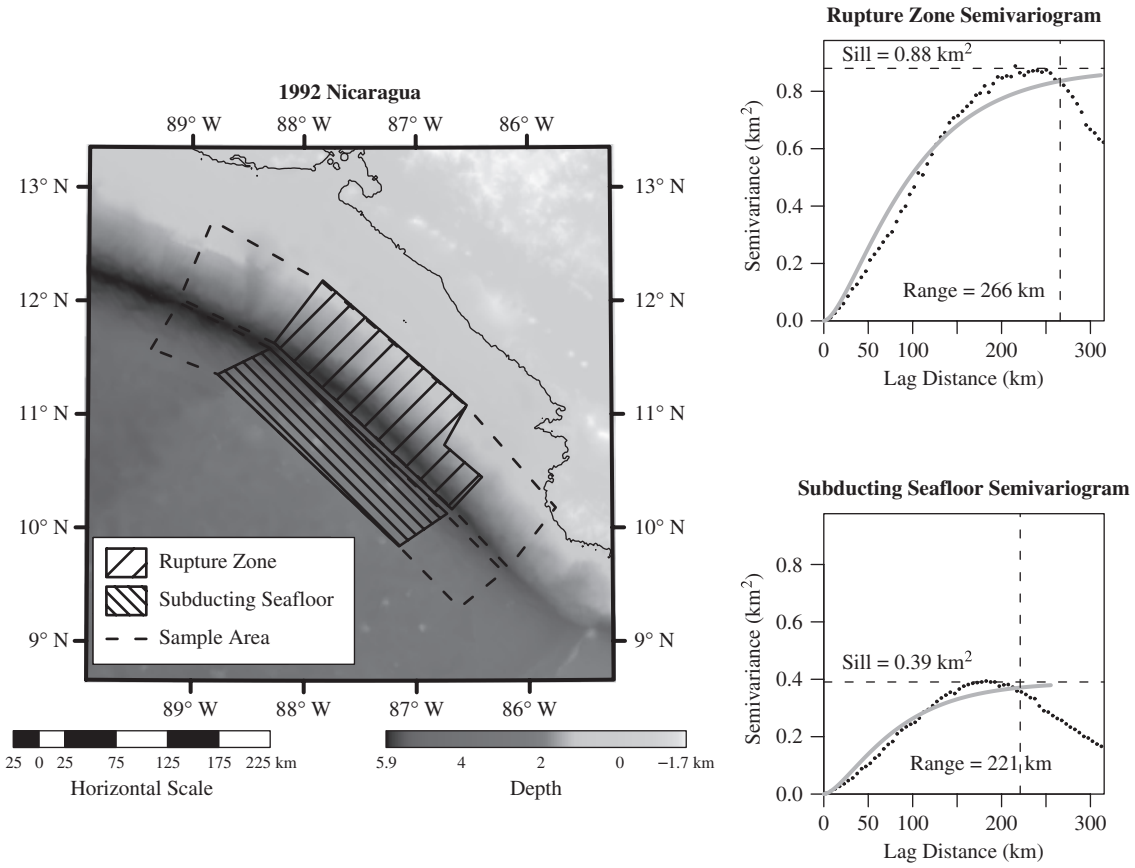

Fig. 2. 1992 Nicaragua rupture zone mapped on the Smith and Sandwell bathymetry data (left panel). The corresponding subducting seafloor section and sample areas used for both forearc and subducting seafloor are mapped as well. The semivariograms constructed from the rupture zone sample area (upper right panel) and subducting seafloor sample area (lower right panel) show fitted Matérn models and derived sills and ranges.

distort the effects that the geomorphological features of interest have in the semivariograms. The lag distance bins for each semivariogram were constructed using a constant bin size of 5 km throughout the study. Therefore, the number of bins for a given semivariogram equals the maximum lag distance divided by 5 km. Also, we included directional constraints that only used pairs oriented in a direction parallel to the trench axis, with a $\pm 5^{\circ}$ tolerance. The tendency of rupture zones to extend parallel to the trench axis suggests that any geomorphological feature influencing seismicity should do so principally as a function of its along-strike dimension.

Models of the Matérn (a.k.a.'von Kármán') family of correlation functions parameterize the sill and range for all semivariograms in this study. Goff & Jordan (1988) validate this model by using it to generate synthetic multibeam sonar data that are statistically similar to actual multibeam sonar data. The Matérn model takes on the generalized form of:

$$\gamma(u) = \tau + \sigma^2\left(1 - \frac{2^{1-\kappa}}{\Gamma(\kappa)}\frac{u^{\kappa}}{\phi^{\kappa}}\mathrm{K}_{\kappa}\left(\frac{u}{\phi}\right)\right) \qquad (2)$$

where u is the midpoint lag distance (mean of the range of L) for each bin, τ is the nugget (variance attributed to noise in the data), σ^2 is the partial sill (variance explained by the distance between data points), ϕ is a scale parameter associated with the range, and K is a modified Bessel function of order κ (Diggle & Ribeiro, 2006). The sill is the sum of the nugget and partial sill, and we determined the range as the lag distance associated with 95% of the sill for each model (Delhomme, 1978; Isaaks & Srivastava, 1989). The *variofit* function of the *geoR* package (made for the open-source data analysis environment *R* (version 2.6.1; R Development Core Team, 2007)) fits this parametric model to the empirical semivariograms using weighted least squares, where the number of pairs in each bin determined the weight for that bin (Ribeiro & Diggle, 2001). We constrained model fitting from the origin of the semivariogram to a lag distance slightly greater than the lag distance associated with the first significant plateau in the semivariogram, and limited κ to $0 < \kappa \leq 1$ to obtain the optimum κ that yielded the least sum of squared residuals [see Table 1 (rupture zones) and Table 2 (subducting seafloor) for model parameter values].

RESULTS

Tables 1 and 2 present results from the semivariogram model fitting, as well as the moment magnitudes, rupture area sizes, and sample sizes for the rupture areas and subducting seafloor sections. These tables are ordered by

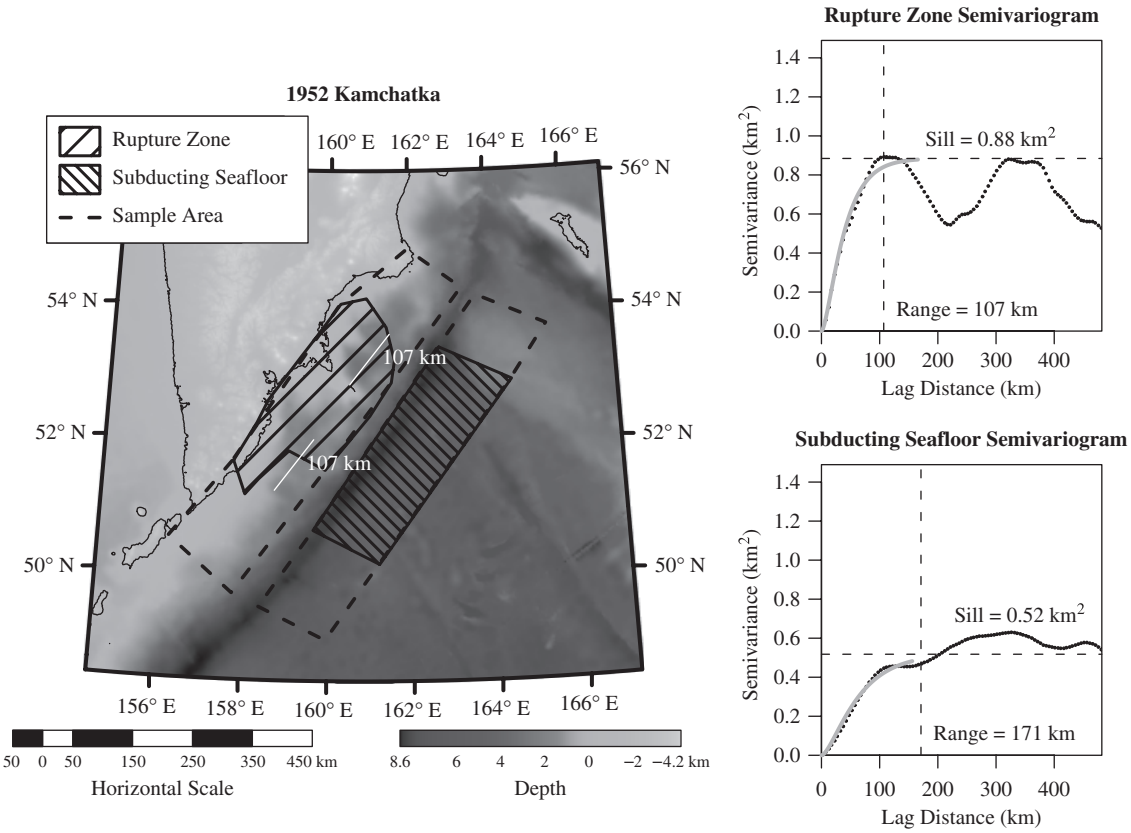

Fig. 3. 1952 Kamchatka rupture zone mapped on the Smith and Sandwell bathymetry data (left panel). The corresponding subducting seafloor section and sample areas used for both forearc and subducting seafloor are mapped as well. The semivariograms constructed from the rupture zone sample area (upper right panel) and subducting seafloor sample area (lower right panel) show fitted Matérn models and derived sills and ranges. White line segments on the map (left panel) are the length of the range determined from the rupture zone semivariogram, and are oriented approximately parallel to the trench axis. Note that they extend roughly from the center of the depressions to the edges.

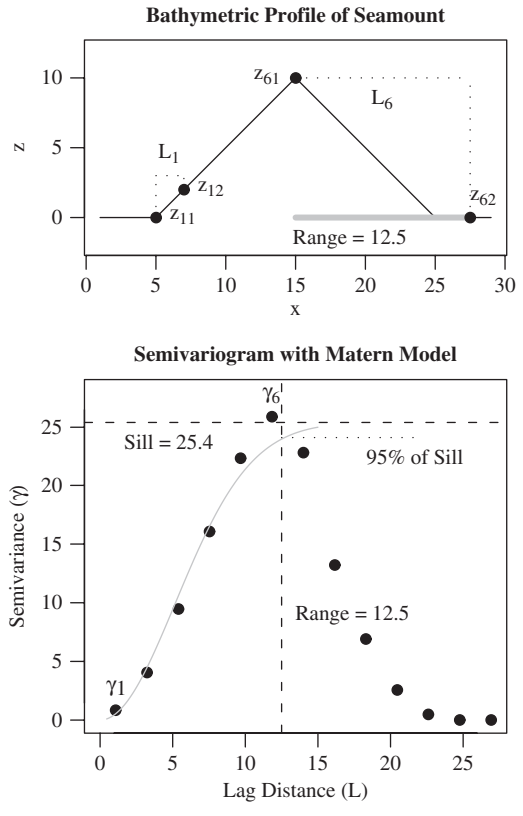

ascending rupture area. We include the maximum lag distance (L_{max}) used to construct the semivariograms as a check on the quality of the range values obtained. A range value close to L_{max} may represent an artificial range created by an L_{max} insufficiently large to constrain the true range.

The range and sill parameters offer a generalized description of the bathymetric geomorphology. The range constitutes the horizontal distance associated with the variance of the sample area, and so in areas dominated by such features as basins, ridges, or seamounts, the range

Fig. 4. A cartoon of an idealized profile across a seamount (top) and corresponding semivariogram (bottom). γ_1 is calculated from every possible pairing of z values separated by a range of small lag distances (z_{11} and z_{12} serve as one example pair separated by h_1; see Eqn (1) in text), and γ_6 is calculated from every possible pairing of z values separated by a range of larger lag distances (z_{61} and z_{62} serve as one example pair separated by L_6). γ_1, γ_6, and all other γ_6 values are plotted against the midpoints of the binned lag distances to make the semivariogram. The Matérn model (gray curve in semivariogram) estimates the sill (maximum semivariance) and range (distance corresponding to 95% of sill). The range has been plotted at the base of the seamount (in gray), and approximates half the basal diameter.

will approximate the horizontal distance from trough to peak [Fig. 3 (note white lines plotted on map that correspond to range) and Fig. 4]. Sill, defined as the variance, will scale to the amount of relief expressed by these dominating features. Note the differences between semivariograms for smooth seafloor from offshore Nicaragua (right panels of Fig. 2) and rough seafloor from Kamchatka (right panels of Fig. 3). The forearc rupture zone sills are approximately equivalent, but the range for the rougher forearc (Kamchatka) is much smaller than that for the smoother forearc (Nicaragua). Comparing the subducting seafloor for these two sites, the rougher seafloor at Kamchatka has both a higher sill (greater relief) and a shorter range (over smaller scale).

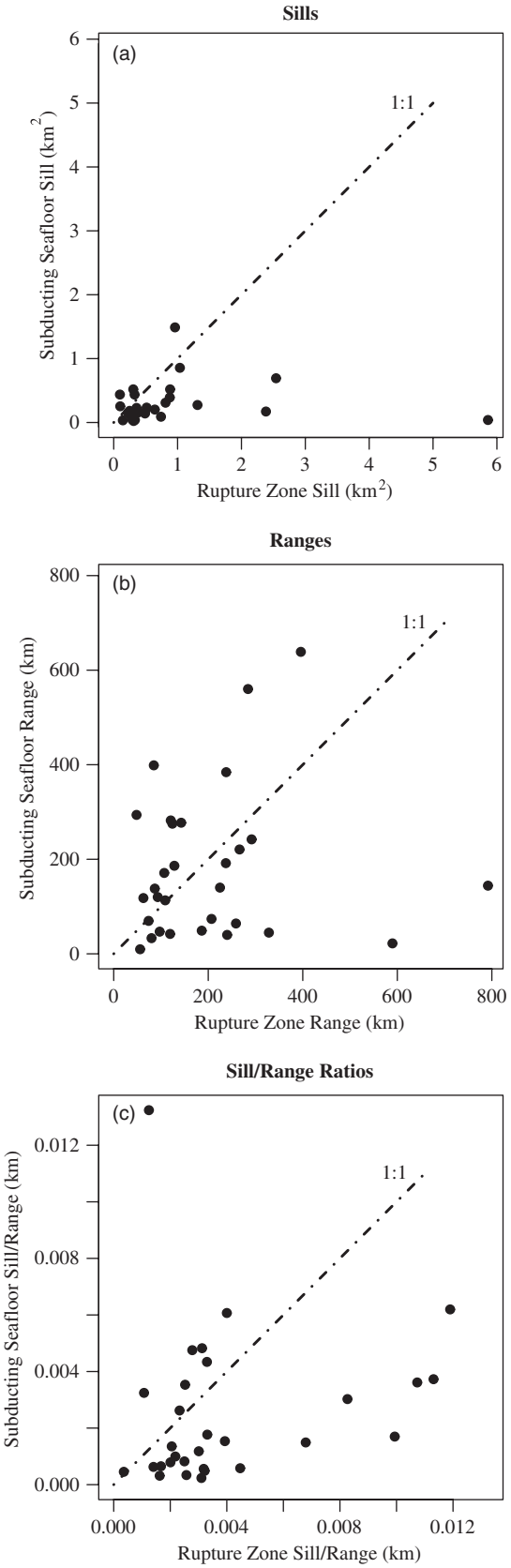

Although the range and sill parameters do not appear particularly correlated between all the rupture zones and subducting seafloor (Fig. 5a and b), the rupture zone values generally seem larger than the subducting seafloor values. Paired *t*-testing, with the null hypothesis that the true mean of rupture zone sills equals the true mean of subducting seafloor sills and the alternative hypothesis that the former exceeds the later, showed that rupture zone sills are statistically larger than subducting seafloor sills (illustrated by the majority of data points in Fig. 5a falling below the 1 : 1 line). For this test, we obtained a *t* statistic of 2.43 with a *P*-value (probability of obtaining a *t* statistic at least as extreme given that the null hypothesis is valid) of 0.01 (see Table 3 for confidence interval values). A *P*-value this low means that rejection of the null hypothesis is reasonable, and rupture zone sills are probably larger than subduction zone sills. The same test run on the range values of the two groups (Fig. 5b) gave a *P*-value of 0.28, indicating that the null hypothesis cannot be rejected in this case.

To examine the 'roughness' of these 60 different sections of bathymetry, we combine the sill and range into a single parameter, following Bell, 1979. Because the sill is the variance in vertical measurements, and range is horizontal distance associated with that variance, the ratio of sill to range is akin to the slope associated with the variance. Specifically, this ratio represents the linear change of bathymetric variance with horizontal distance, up to the maximum variance. A higher sill to range ratio indicates bathymetry with greater variability over shorter distances, which we will consider as rougher than a surface with a smaller ratio. To investigate any relationship between forearc and subducting seafloor roughness, we plot the ratios from the former terrain with those from the latter (Fig. 5c). For the rupture zones, larger ratios (rougher) correspond to steeper basins with greater relief, while smaller ratios (smoother) correspond to shallower and/or longer basins, or perhaps no basins at all. In the subducting seafloor environment, larger ratios indicate steeper features (seamounts, ridges, etc.), perhaps with greater spatial frequency, and smaller ratios indicate

Fig. 5. Comparison of sill (a) and range (b) values, as well as the ratio of the two (c), from rupture zone and subducting seafloor semivariogram modeling. While (a) and (c) show larger values for the rupture zones than for the subducting seafloor (most points lie below 1 : 1 line; see Table 3 for *t*-test results), no correlation of parameters is observed.

Table 3. Results of *t*-tests

		t Statistic	*P*-value	Mean	95% confidence interval	
Rupture sills vs. Subducting sills	Figure 5a	2.43	0.01085	0.508	0.1521	Inf
Rupture ranges vs. Subducting ranges	Figure 5b	0.58	0.28347	22.767	-44.0227	Inf
Rupture ratios vs. Subducting ratios	Figure 5c	2.14	0.02029	0.001	0.0003	Inf
Subducting ratios vs. Synthetic ratios	Figure 6c	4.94	0.00001	0.739	0.4851	Inf

In all cases, we test that the mean of former group (i.e. rupture sills, rupture ranges, rupture ratios, and subducting ratios) exceeds the mean of latter group (i.e., that the difference between these two means is greater than 0). Therefore, we use one-tailed *t*-tests, where rejection of the null hypothesis is safe when the *P*-value <0.05 (our α value, since we test at 95% confidence) and the lower bound on the confidence interval >0 (hence the infinite values for the upper limits).

shorter and/or longer features, or a lack of features. Paired *t*-testing of the sill to range ratio values gave a *P*-value of 0.02, indicating that the rupture zone ratios are significantly larger than the subducting seafloor ratios (Table 3).

While we identify no convincing correlation between the geomorphology of rupture zones and that of their accompanying subducting seafloor sections, we do observe interesting relationships between the geomorphology of these areas and seismicity (Fig. 6 (subducting seafloor) and Fig. 7 (rupture zones)). While subducting seafloor sill (Fig. 6a), rupture zone sill (Fig. 7a), and rupture zone range (Fig. 7b) all show no legitimate correlation with moment magnitude, subducting seafloor range shows a significant logarithmic correlation with moment magnitude (Fig. 6b). Points in these plots have been classified into an arbitrary number of three groups in terms of the ratio of range to $L_{\max}$ in order to express their trustworthiness, with ratios $\leq 1/3$ being the most reliable. Range measurements approaching $L_{\max}$ may be improperly constrained, and thus the true range may be underestimated. Removing the least reliable data points (with range to $L_{\max}$ ratios $>2/3$) greatly improves the correlation in Fig. 6b, with the R^2 increasing from 0.13 with all the data to 0.44. However, it should be noted that the true range for these several data points, if reliably determined, may exceed the values presented, in which case the correlation in Fig. 6b would diminish.

Although the sill to range ratios for the subducting seafloor and rupture zones have no evident correlation to moment magnitude, both Fig. 6c (rupture zones) and Fig. 7c (subducting seafloor) show decreasing moment magnitude and variance in moment magnitude with increasing roughness (increasing sill to range ratio). This trend suggests that given the geomorphology of a section of forearc or subducting seafloor, one should expect a maximum possible magnitude for an event at that site based on the distribution of magnitudes for sites of similar geomorphology. To express this distribution of maximum events, linear envelope curves denoting these maxima are fit to the data by linearly optimizing:

$$\min \sum_{i=1}^{n} [y_i - (a + bx_i)]^2$$

subject to:

$$y_i - (a + bx_i) \leq 0 \quad \forall i \tag{3}$$

(Vogel *et al.*, 2007). The function *constrOptim* of *R*'s *stats* package solved this constrained optimization problem for the parameters *a* and *b*.

Cloos (1992) provides dimensions for theoretical seamounts associated with specific moment magnitudes. We ran our semivariogram algorithm on synthetic bathymetry containing single seamounts with these dimensions in order to relate them to our results (see Table 4 for seamount data and results). The sill to range ratios of these seamounts are plotted on Fig. 6c alongside our data, and a logarithmic trend line fits the seamount data very well (dotted line). A large majority of our data points fall above the synthetic seamount curve, indicating larger earthquake events than predicted by a model of singular subducting seamounts. To test the significance of this curve as a lower bound, we ran a *t*-test on the residuals of our data with the alternative hypothesis that the true mean of the residuals is positive (i.e. that the data lie above the curve), and obtained a *t* statistic of 4.94 with a *P*-value of 1.5e-5, which means that it is highly unlikely to achieve the same result if the mean of the residuals is less than or equal to zero (Table 3).

DISCUSSION

Although paired *t*-testing showed that the forearc likely possesses larger sills and sill to range ratios than the subducting seafloor, our data show no discernable correlation between subducting seafloor and forearc geomorphology (Fig. 5). We speculate that this lack of correlation comes from the lack of expression of certain forearc basins in the bathymetry data. We expected many of the measurements in Fig. 7a and c to be rougher (greater sills and thus greater ratios), given the basin-centered asperities of Wells *et al.* (2003) and the TPGA and TPTA of Song & Simons (2003). Sediment in-filling of some basins drastically reduces the sill of such bathymetry. This has occurred, for instance, at the Kanto basin (Wells *et al.*, 2003), where little relief is seen in the bathymetry data, and more seen in the free-air gravity data. Therefore, we feel that perhaps

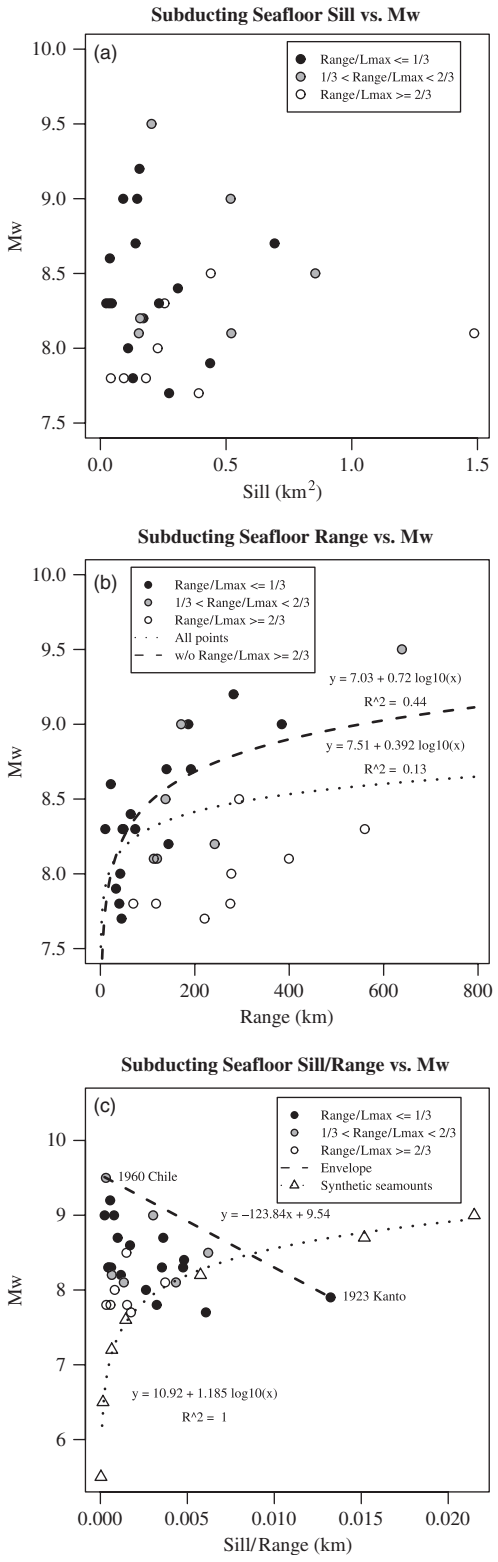

Fig. 6. M_w plotted against sill (a), range (b), and sill/range (c) for the subducting seafloor. For each plot, the data points are classified based on the binning of the ratios of range to L_{max} into three bins. Lower ratios (black circles) indicate better constraint of the sill and range parameters by the models. Logarithmic curves are fit to the data points in (a) and (b), where the dashed line in (b) is only fit to the data points with range/$L_{max} \leq 2/3$. (c) An exceedence envelope (dashed line) is fit to show maximum likely earthquakes, and the dotted line is the log curve regressed to the synthetic seamount data.

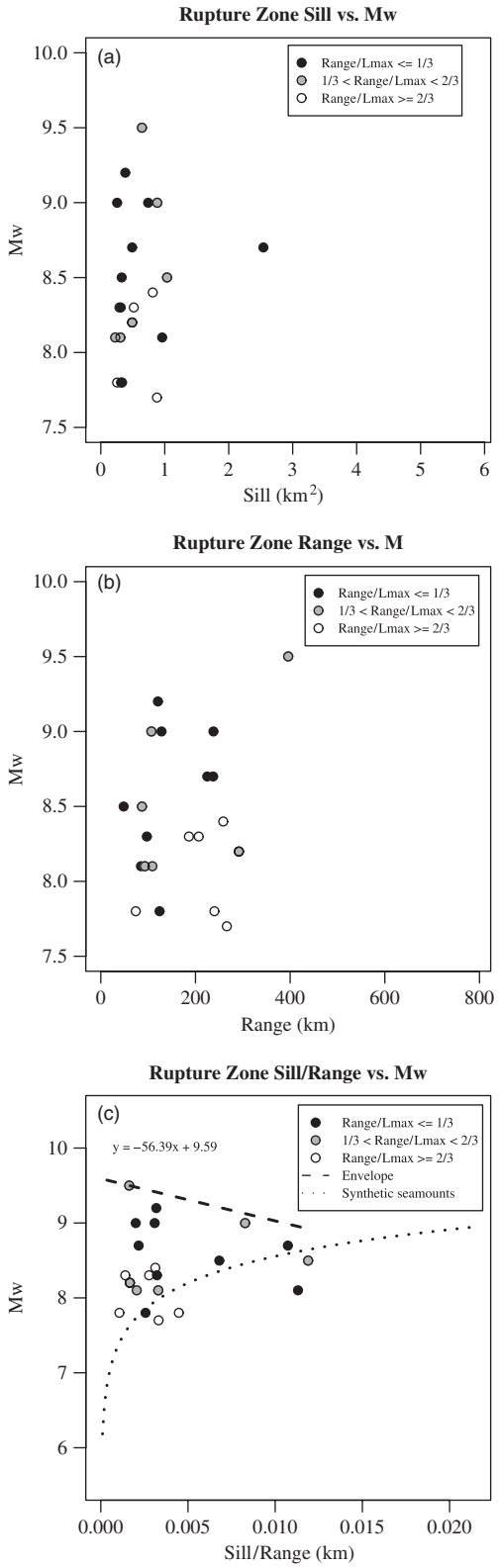

Fig. 7. M_w plotted against sill (a), range (b), and sill/range (c) for the rupture zones. Again, the data points are classified based on the binning of the ratios of range to L_{max} into three bins. Linear and logarithmic curves are fit to the data points in (a) and (b), to illustrate the lack of correlation of these parameters with M_w (c) An exceedence envelope (dashed line) is fit to show maximum likely earthquakes constrained by the rupture zone data, and the dashed line is the exact same synthetic seamount regression as in Fig. 6c.

Table 4. Synthetic seamount dimensions and semivariogram analysis results

Height (km)*	Basal diameter (km)*	M_w*	Rupture area (km^2)	Sill (km^2)	Range (km)	κ	Sum of squares (km^4)
0.4	1.4	5.5	160	0.0004	13	0.10	1
0.7	5.0	6.5	920	0.0030	20	0.31	5
1.3	14.0	7.2	3100	0.0248	38	0.45	95
1.9	23.0	7.6	6200	0.0700	48	0.63	539
3.6	53.0	8.2	17 700	0.4548	79	1.00	21 599
6.1	103.0	8.7	42 000	2.0338	134	1.00	1 135 754
7.8	146.0	9.0	71 000	3.8913	181	1.00	5 793 982

*Height, basal diameter, and M_w values taken from Cloos (1992).

gravity data would be more appropriate than bathymetry data for assessing the characteristics of forearc basins.

Processes related to the subduction of geomorphological features (especially seamounts) and sediment of variable thickness explain the distribution of roughness data points for the subducting seafloor sections in Fig. 6b and c. Seamounts and ridges effectively control the size of asperities and may establish characteristic earthquakes at particular sections of subduction zones (Bilek *et al.*, 2003). Cloos (1992) shows that, on average, taller seamounts with larger basal diameters correspond to larger magnitude events. Our sill measurements do not support this observation, as no correlation can be observed with moment magnitude (Fig. 6a), but the logarithmic correlation between subducting seafloor range and moment magnitude does support it (Fig. 6b). A logarithmic trend between range and moment magnitude seems plausible, especially when considering that moment magnitude is classically defined as a function of the logarithm of rupture area (Kanamori, 1977). The relatively stronger correlation of subducting seafloor range to moment magnitude than sill to moment magnitude suggests that the horizontal dimension parallel to the trench axis of subducting features controls seismicity more than the height. However, overlying sediment may be significantly and variably reducing the sill measurements, such that the roughness of the subducting crust is not expressed in our measurements.

The variance in magnitude observed in smoother subducting seafloor and distribution of sill to range ratios above the synthetic seamount curve may be a function of sediment thickness. Thatcher (1990) proposes a scenario for large ruptures where multiple areas of high moment release are separated by weak zones of low shear strength. With stress concentrated at the asperities, a dynamic rupture process may originate at one asperity and spread to the other asperities, with slip occurring relatively easily along the intermediate low-shear-strength zones. These zones would effectively link the high-strength zones (asperities) into one, large composite rupture. We propose that smooth subducting seafloor would be conducive to these large magnitude earthquakes, with bathymetric highs (such as seamounts and ridges) acting as the asperities and areas of thick sediment layers in between these features providing the low shear strength. Thinner sediment layers and shorter bathymetric features generate similar ratios of sill to range (are just as smooth), but will not rupture so extensively because less stress is needed to rupture the shorter, less wide seamounts. Because the synthetic seamounts do not include sediment cover, data points lying closer to this curve should represent seafloor with thin sediment, while those further away represent thicker sediment relative to the height of the subducting feature ['relative' is used here because we consider variance of depth (sill) in this study]. Consider a seamount that, when sheared during subduction, generates a specific moment magnitude. Partial burial of that same seamount will greatly reduce the measured sill and somewhat reduce the measured range, yielding a smaller (i.e. smoother) sill to range ratio, but still the same moment magnitude should be generated. Therefore, the upper envelope curve may represent the decrease in maximum magnitude with decreasing sediment thickness relative to feature height.

The sill to range ratio data support this hypothesis when examined more closely. Consider two end-member cases: the 1960 Chile and 1923 Kanto events, both of which happen to lie close to or on the upper envelope curve (Fig. 6c). The 1960 Chile event has the largest magnitude, and the geomorphology of the subducting seafloor is quite smooth, with sediment filling the trench and no prominent seamounts, ridges, or grabens being subducted. A series of parallel fracture zones in the subducting plate indicate seismic segmentation of the margin (Barrientos & Ward, 1990). These fractures constitute bathymetric lows, so it is likely that coupling takes place between the sections of elevated subducting seafloor between these fractures. Areas of high slip are centered on basins overlying the locations where these intermediate sections of seafloor would couple with the overriding plate (Wells *et al.*, 2003), with the amount of slip decreasing with distance south of the epicenter. On the other hand, the 1923 Kanto event is strictly confined to a single asperity located at the subduction of the large Izu-Bonin arc.

Rupture zone roughness measurements constrain a maximum moment magnitude envelope (Fig. 7c) similar to that of the subducting seafloor, but we feel that the subducting seafloor curve is more reliable. Curiously, both envelope curves intercept the *y*-axis at similar values of moment magnitude (indicating a maximum magnitude of 9.54–9.59), but have dissimilar slopes. The envelope fit to the subducting seafloor measurements shows a steeper trend, indicating better correlation with the data points. In the forearc basins, sediment filling hinders meaningful measurements of sill and range, whereas it becomes necessary to represent sediment accumulation in the subducting seafloor measurements because of the role it plays in rupture dynamics. Additionally, we observe a correlation between moment magnitude and subducting seafloor range, but no such correlation with rupture zone sill or range. To address a possible lower bound on the rupture zone roughness measurements, we plot the synthetic

 Basin Research, 10.1111/j.1365-2117.2008.00368.x

seamount curve from Fig. 6c on Fig. 7c (dotted line). This curve merely proposes that forearc basins may possibly constrain the minimum magnitude events. For a certain basin, we expect a certain magnitude event, but sediment in-filling of that basin will greatly reduce its sill and sill to range ratio.

CONCLUSION

We found that the size of subduction zone earthquakes relates to the scale of the roughness elements on the incoming plate. While the adjacent forearc is often rougher than the incoming plate, it does not have the same systematic correlation with earthquake magnitude. We cannot conclude that the similar distributions seen in Figs 6c and 7c represent a relationship between subducting seafloor geomorphology and forearc basins because of the lack of correlation between forearc rupture zone and subducting seafloor parameters throughout Fig. 5. This does not eliminate subduction erosion as a mechanism linking subducting geomorphology and forearc geomorphology, but it does not enforce it, and suggests to us that other types of data besides bathymetry need to be analyzed to assess the relationship.

Moment magnitude of subduction zone rupture events are best constrained by the bathymetric roughness of subducting seafloor. Careful model fitting to sample semivariograms provides meaningful parameters for quantifying geomorphology. The ratio of the sill and range parameters describes the roughness of bathymetry, where roughness in this case is considered as the amount of relief per distance. For the subducting seafloor, the distribution of our roughness measurements meaningfully reflects the differences in geology between regions. Plotting moment magnitude of the 30 events in this study against the subducting seafloor roughness measurements, we see a decline in maximum magnitude with increasing roughness. Rougher seafloor possesses significant bathymetric highs that serve as rupture asperities, but does not possess low-shear-strength sediment between bathymetric highs. Such sediment aids in rupture propagation, and also diminishes the sill measurements of bathymetric features. Wider bathymetric highs generate wider asperities, and thus greater earthquakes. Bathymetry containing wide features and thick sediment appears relatively smooth, however smooth bathymetry may also contain very little sediment and small features, which generate smaller earthquakes. This is the reason for the large variance in magnitude associated with smoother bathymetry seen in Fig. 6c. The analysis of synthetic seamount data from Cloos (1992) suggests that subducting terrain containing a single seamount with no sediment cover may constitute a lower bound of possible magnitudes for seafloor of a given roughness.

ACKNOWLEDGEMENTS

This research was funded by the National Science Foundation under Grant OISE-0530151 and the Tufts University Dean's Fellowship Program. We would like to thank Guy Simpson and Alexander Densmore for initiating this study during Brian McAdoo's stay with the ETH-Zurich's Basin Analysis group, lead by Philip Allen. Additionally, the authors thank John Goff (UTIG) and Jeff McGuire (WHOI) for the practical advice given during review of this paper, and Eric Thompson (Department of Civil and Environmental Engineering, Tufts University) for all of his help.

REFERENCES

Barrientos, S.E. & Ward, S.N. (1990) The 1960 Chile earthquake: inversion for slip distribution from surface deformation. *Geophys. J. Int.*, **103**, 589–598.

Bell, T.H. (1979) Mesoscale sea floor roughness. *Deep-Sea Res.*, **26A**, 65–76.

Bilek, S.L. (2007) Using earthquake source durations along the Sumatra-Andaman subduction system to examine fault-zone variations. *Bull. Seismol. Soc. Am.*, **97**(1), S62–70.

Bilek, S.L. & Lay, T. (1999) Rigidity variations with depth along interplate megathrust faults in subduction zones. *Nature (London)*, **400**, 443–446.

Bilek, S.L., Schwartz, S.Y. & DeShon, H.R. (2003) Control of seafloor roughness on earthquake rupture behavior. *Geology (Boulder)*, **31**, 455–458.

Bishop, M.P., Shroder, J.F. Jr & Colby, J.D. (2003) Remote sensing and geomorphometry for studying relief production in high mountains. *Geomorphology*, **55**, 345–361.

Byrne, D.E., Davis, D.M. & Sykes, L.R. (1988) Loci and maximum size of thrust earthquakes and the mechanics of the shallow region of subduction zones. *Tectonics*, **7**, 833–857.

Carr, J.R. (1995) *Numerical Analysis for the Geological Sciences*, lst edn. Prentice Hall, Englewood Cliffs, NJ.

Carr, J.R. (1997) Statistical self-affinity, fractal dimension, and geologic interpretation. *Eng. Geol.*, **48**, 269–282.

Carr, J.R. & Benzer, W.B. (1991) On the practice of estimating fractal dimension. *Math. Geol.*, **23**, 945–958.

Cloos, M. (1992) Thrust-type subduction-zone earthquakes and seamount asperities; a physical model for seismic rupture. *Geology (Boulder)*, **20**, 601–604.

Cloos, M. & Shreve, R.L. (1996) Shear-zone thickness and the seismicity of Chilean- and Marianas-type subduction zones. *Geology (Boulder)*, **24**, 107–110.

Delhomme, J.P. (1978) Kriging in the hydrosciences. *Adv. Water Resources*, **1**, 251–266.

Diggle, P.J. & Ribeiro, P.J. (2006) *Model-based Geostatistics*, lst edn, Springer Series in Statistics, Springer, New York.

Fuller, C.W., Willett, S.D. & Brandon, M.T. (2006) Formation of forearc basins and their influence on subduction zone earthquakes. *Geology*, **34**(2), 65–68.

Glenn, N.F., Streutker, D.R., Chadwick, D.J., Thackray, G.D. & Dorsch, S.J. (2006) Analysis of lidar-derived topographic information for characterizing and differentiating landslide morphology and activity. *Geomorphology*, **73**, 131–148.

Goff, J.A. & Jordan, T.H. (1988) Stochastic modeling of seafloor morphology: inversion of sea beam data for second-order statistics. *J. Geophys. Res.*, **93**(B11), 13589–13608.

Goff, J.A., Orange, D.L., Mayer, L.A. & Hughes-Clarke, J.E. (1999) Detailed investigation of continental shelf morphology using a high-resolution swath sonar survey; the Eel

Margin, Northern California; the formation of continental-Margin Strata. *Mar. Geol.*, **154**, 255–269.

Isaaks, E.H. & Srivastava, M.R. (1989) *An Introduction to Applied Geostatistics*, lst edn. Oxford University Press, New York.

Kanamori, H. (1977) The energy release of great earthquakes. *J. Geophys. Res.*, **82**, 2981–2987.

Kanamori, H. (1986) Rupture processes of subduction zone earthquakes. *Ann. Rev. Earth Planet. Sci.*, **14**, 293–322.

Kanamori, H. & Kikuchi, M. (1993) The 1992 Nicaragua earthquake: a slow earthquake associated with subducted sediments. *Nature*, **361**, 714–716.

Laursen, J., Scholl, D.W. & von Huene, R. (2002) Neotectonic deformation of the central Chile margin; deepwater forearc basin formation in response to hot spot ridge and seamount subduction. *Tectonics*, **21**(5), #1038, 27pp.

Llenos, A.L. & McGuire, J.J. (2007) Influence of fore-arc structure on the extent of great subduction zone earthquakes. *J. Geophys. Res.*, **112**, #B09301, 31pp.

McAdoo, B.G., Capone, M.K. & Minder, J. (2004) Seafloor geomorphology of convergent margins: implications for Cascadia seismic hazard. *Tectonics*, **23**(6), #TC6008, 15pp.

Mogi, K. (1969) Relationship between the occurrence of great earthquakes and tectonic structures. *Bull. Earthquake Res. Inst.; Tokyo Daigaku Jishin Kenkyusho Iho*, **47**, 429–451.

R Development Core Team (2007) R: A language and environment for statistical computing. *R Foundation for Statistical Computing, Vienna, Austria*. ISBN: 3-900051-07-0. http://www.R-project.org

Ribeiro, P.J. & Diggle, P.J. (2001) geoR: A package for geostatistical analysis. *R-News*, **1**(2). http://cran.r-project.org/doc/Rnews

Satake, K., Wang, K. & Atwater, B.F. (2003) Fault slip and seismic moment of the 1700 Cascadia earthquake inferred from Japanese tsunami descriptions. *J. Geophys. Res.*, **108**(B11), #2535, 17pp.

Smith, W.H.F. & Sandwell, D.T. (1997) Global seafloor topography from satellite altimetry and ship depth soundings. *Science*, **277**, 1956–1962.

Song, T.A. & Simons, M. (2003) Large trench-parallel gravity variations predict seismogenic behavior in subduction zones. *Science*, **301**, 630–633.

Spence, W., Mendoza, C., Engdahl, E.R., Choy, G.L. & Norabuena, E. (1999) Seismic subduction of the Nazca ridge as shown by the 1996–97 Peru earthquakes; Seismogenic and Tsunamigenic processes in shallow subduction zones. *Pure Appl. Geophys.*, **154**, 753–776.

Sugiyama, Y. (1994) Neotectonics of southwest Japan due to the right-oblique subduction of the Philippine Sea plate. *Geofis. Int.*, **33**, 53–76.

Sung, Q.-C. & Chen, Y.-C. (2004) Self-affinity dimensions of topography and its implications in morphotectonics; an example from Taiwan. *Geomorphology*, **62**, 181–198.

Tanioka, Y., Ruff, L. & Satake, K. (1997) What controls the lateral variation of large earthquake occurrence along the Japan Trench? *Island Arc*, **6**, 261–266.

Thatcher, W. (1990) Order and diversity in the modes of circum-Pacific earthquake recurrence. *J. Geophys. Res.*, **95**, 2609–2623.

Vogel, R.M., Matalas, N.C., England, J.F. & Castellarin, A. (2007) An assessment of exceedence probabilities of envelope curves. *Water Resources Res.*, **43**, W07403.

von Huene, R. & Scholl, D.W. (1991) Observations at convergent margins concerning sediment subduction, subduction erosion, and the growth of continental crust. *Rev. Geophys.*, **29**, 279–316.

Wells, R.E., Blakely, R.J., Sugiyama, Y., Scholl, D.W. & Dinterman, P.A. (2003) Basin-centered asperities in great subduction zone earthquakes; a link between slip, subsidence, and subduction erosion? *J. Geophys. Res.*, **108**(B10), #2507, 30pp.

Manuscript received 23 September 2007; Manuscript accepted 15 May 2008.

